# EXPERIMENTAL STUDY OF TURBULENT OSCILLATORY BOUNDARY LAYERS IN A NEW OSCILLATORY WATER TUNNEL

Jing Yuan[1], Ole Secher Madsen[2] and Eng Soon Chan[3]

A new oscillatory water tunnel has been built in the Civil and Environmental Engineering Department's Hydraulic Laboratory at the National University of Singapore. It can accurately produce oscillatory flows that correspond to full-scale sea waves. Tests including pure sinusoidal waves and combined wave-current flows over smooth and rough bottoms have been performed. High quality measurements of the boundary layer flow fields are obtained using a PIV system. The PIV measured flow field is phase and spatially averaged to give a mean vertical velocity profile. It is found that the logarithmic profile can accurately approximate the near-bottom first-harmonic amplitude of sinusoidal waves and give highly accurate determinations of the hydrodynamic roughness and the theoretical bottom location. The bottom shear stress obtained from momentum integral is in general agreement with results from log-profile fitting. The current profiles of combined wave-current flows indicate a two-log-profile structure as suggested by simple combined wave-current flow theory. The difference between the two current shear velocities obtained from combined wave-current flows, as well as a small but meaningful third harmonic embedded in a pure sinusoidal wave, suggest the existence of a time-varying turbulent eddy viscosity.

*Keywords: Oscillatory water tunnel; turbulent wave and wave-current boundary layers; logarithmic profile*

## INTRODUCTION

Sediment transport is of primary interest in coastal engineering. In coastal regions, waves and currents are generally present simultaneously. The waves are usually stronger and have a thinner boundary layer, so they generally act as the main mechanism in mobilizing the bottom sediments. The co-existing current, even if weak, can therefore create a net sediment transport in its direction. Thus, accurate prediction of sediment transport processes in coastal regions requires a delicate understanding of the bottom boundary layer hydrodynamics associated with waves and combined wave-current flows.

Usually, the boundary layer flow under a surface wave which can induce noticeable amounts of sediment transport is in the regime of fully developed rough turbulent flow, e.g., the boundary layer under episodic storm waves. The near-bottom wave orbital velocity amplitude $U_{bm}$ can reach the order of m/s, so this type of wave boundary layer flow can have a Reynolds number $RE=A_{bm}U_{bm}/\nu$ up to $O(10^6)$, where $A_{bm}$ is the excursion amplitude and $\nu$ is the water molecular viscosity. Previous experimental studies of the oscillatory boundary layer are mostly conducted using two types of facilities, wave flumes and oscillatory wave tunnels (OWT). To generate prototype flow conditions of such high Reynolds numbers, the laboratory wave flume has to be very large. For example, the large wave flume in Hanover (Dohmen-Janssen and Hanes, 2002) is 280m long, 7m deep and 5m wide. Therefore, it will be very cumbersome to set up experiments and deploy instruments for velocity measurements such as PIV. However, the OWT has much smaller size compared to the large wave flume but can still generate oscillatory flows of the same Reynolds numbers. For example, the Deltares OWT is only 12m long, 30cm wide and 80cm deep (Dohmen-Janssen et al., 2001). The convenience in setting up experiments and deploying various measurement instruments makes the OWT an excellent experimental facility for studies of oscillatory boundary layer hydrodynamics. Some experimental studies have been done using OWTs, e.g., Jonsson and Carlsen (1976), Hino et al. (1983), Sleath (1987), Jensen et al. (1989), Dohmen-Janssen et al. (2002) and van der A et al. (2011). However, experiments with high quality measurements and well-defined bottom roughness configurations are still lacking, especially for combined wave-current boundary layers. In this paper, high quality experiments on the wave and wave-current boundary layer hydrodynamics using a new OWT are presented.

[1] Graduate student, R. M. Parsons Laboratory 48-208, MIT, Cambridge, MA 02139, USA.
[2] Donald and Martha Harleman Professor of Civil and Environmental Engineering, R. M. Parsons Laboratory 48-216C, MIT, Cambridge, MA02139, USA.
[3] Professor and Dean of the Faculty of Engineering, NUS, Block EA #07-26, 9 Engineering Drive 1, Singapore 117576

## EXPERIMENTAL SETUP

### The OWT

A new OWT has been built in the Hydraulics Laboratory of the Civil and Environmental Department and the National University of Singapore. Following the general design concepts of the Deltares OWT, the main part is a 10m-long test section with a 50cm-deep and 40cm-wide rectangular cross section and glass sidewalls and acrylic lids along its entire length (Figure 1a and b). A 20cm-deep trough, intended for future experiments involving sediments, is currently fitted with wooden false bottom blocks, seen Figure 1b. Two 1m-diameter stainless steel vertical cylindrical risers are located at the ends of the test section. One contains a programmable, hydraulically actuated piston, manufactured by MTS, to generate prescribed oscillatory (regular or random) wave motions, and the other is open to the atmosphere. A force cell attached to the piston, Figure 1c, gives instantaneous measurements of the driving force on the piston, which is used to trigger emergency shut-down when exceeding the design limit. However, preliminary analyses of force measurements suggest that these are sufficiently accurate and repeatable to potentially be used to estimate the bottom shear force exerted on the flow in the test section. The oscillatory flow design limits for excursion, velocity, and acceleration in the test section are 2m, 2m/s and 2m/s$^2$, respectively, for periods 2s<$T$<12s. The transparent sidewalls and lid facilitate non-intrusive velocity measurements by a dedicated 2D Particle Image Velocimetry (PIV) system. The measurement window can be either vertical or horizontal and located at any lateral or longitudinal position of the test section. PIV measurements near the riser-ends show that the inflow into the test section after passing through a honeycomb filter is uniform. A current generation system has been built to superimpose a current on oscillatory flows. The core part is a Börger EL1550 Rotary Lobe pump which can produce a current of up to 50cm/s average velocity in the test section. The direction of the current can be easily reversed by simply reversing the pump's rotation. The current enters or leaves the main test channel through flexible telescoping connections, Figure 1d, allowing the entire facility to be tilted, up to a slope of 1 on 20, with the current generation system operating. Thus, it will be possible to simulate sediment transport associated with combined wave-current boundary layer flows on a sloping bottom in this facility. To the authors' knowledge, experiments of this type have never been done before.


**Figure 1. Pictures of the OWT: (a) the transparent lid, (b) the main test channel, (c) the force transducer, (d) the flexible telescoping connections**

To test whether the piston can precisely generate a specified oscillatory motion, several preliminary tests with smooth bottom were performed. The piston velocity is measured and converted into a cross-section average velocity $U_{piston}$ inside the test channel. This is to be compared with the PIV measured free-stream velocity $U_{piv}$. Since the smooth turbulent boundary layer is very thin, these two velocities should be very close to each other. Table 1 shows the comparison based on a test which is almost at the design limits of the OWT. The target velocity $U_{target}$, i.e., the command signal input, is specified as:

$$U_{\text{target}}(t) = U_1 \cos(\omega t) + U_2 \cos(2\omega t + \varphi_2) \quad (1)$$

where $U_1$ and $U_2$ are the amplitudes of the first and second harmonics and $\varphi_2$ is the phase lead of the second harmonic. The measurement shows that the first and second harmonic amplitudes of $U_{piston}$ deviate from those of $U_{target}$ by only 0.02cm/s and 0.6cm/s, respectively. The phase lead of the second harmonic deviates from the target by only about 5 degrees. This phase difference can be further corrected by adjusting the input signal, i.e., subtracting about 5 degrees from the $\varphi_2$ of input signal. The measured third harmonic is also negligibly small. These results indicate that the system can perfectly produce a specified piston motion. The difference between $U_{piston}$ and $U_{piv}$ is only about 0.5cm/s in amplitudes and 0.2 degree in phase, which shows excellent flow response to the piston motion. Therefore, the system can precisely produce a specified oscillatory motion with an extremely high accuracy.

**Table 1. The flow response to the piston motion**

| | $U_1$[cm/s] | $U_2$[cm/s] | $U_3$[cm/s] | $\varphi_2$ [°] |
|---|---|---|---|---|
| $U_{target}$ | 157.08 | 39.27 | 0 | 0 |
| $U_{piston}$ | 157.06 | 39.84 | 2.43 | -5.56 |
| $U_{piv}$ | 157.52 | 39.50 | 2.41 | -5.42 |

**PIV measurements**

The 2D near-bottom velocity field along the lateral center line of the OWT is measured using a PIV system, supplied by TSI. The measured area is located around the longitudinal center of the test channel, so the effect of the inlet and outlet is reduced to a minimum. The flow field is illuminated using a double-pulsed YAG 135-15 Litron Nano L laser. The laser is spread into a thin laser sheet by a set of spherical and cylindrical lenses, and then introduced into the test channel through the transparent lid. The laser sheet is aligned with the centerline of the test channel. The illuminated flow field near the bottom is captured by a Powerview 4M Plus 2000-by-2000 pixels high speed camera at 5.12Hz (the maximum frequency is 7.5Hz). The firing of laser and the capturing of images by the camera are synchronized by a 610035 LaserPulse Synchronizer. During all tests, the instant when PIV measurements start is marked on the time series of the piston motion measurements using a National Instruments PXIe-8133 controller, so the PIV and piston motion measurements are synchronized.

The resolution is about 50μm/pixel for most of the tests. The corresponding measured area is about 10cm-by-10cm. Only for the tests with strongest wave, e.g., the test SP400Ar in Table 2, 10cm is not enough to cover the entire boundary layer. For such cases, additional tests with coarser resolution (100μm/pixel) are conducted. The PIV image is processed using the Insight4G supplied by TSI. Since the flow is generally parallel to the bottom, there is no mean velocity in the vertical direction but just turbulent fluctuations. Consequently, the size of interrogation grid for cross-correlation analysis is chosen to be 128(horizontal)-by-16(vertical) pixels, corresponding to a physical size about 6.4mm-by-0.8mm (12.8mm-by-1.6mm for coarser resolution). Before processing the PIV images, the mean background is removed to enhance the signal-to-noise ratio. After processing the images, a local-median validation is applied to the obtained velocity vectors to remove erroneous vectors. Rejected vectors are replaced by the local median.

The obtained time series of near-bottom flow field is first averaged at each individual phase of the oscillatory movement to give the phase-averaged velocity field:

$$\hat{\theta}(x, y, t) = \frac{1}{N}\sum_{n=1}^{N}\theta(x, y, t + (n-1)T) \quad 0 < t < T \quad (2)$$

where $x$ is the horizontal coordinate, $y$ is the vertical coordinate of which the origin is set to the top of the bottom roughness elements (Figure 2), $t$ is time, $N$ is the total number of periods, $T$ is the wave period and $\theta$ is the velocity component ($u$ or $w$). The phase-averaged velocity field is then spatially averaged:

$$<\hat{\theta}>(y, t) = \frac{1}{M}\sum_{m=1}^{M}\frac{1}{N}\sum_{n=1}^{N}\theta(x_m, y, t + (n-1)T) \quad 0 < t < T \quad (3)$$

where $M$ is the total number of $x$-locations. Since the flow field is homogenous in the longitudinal direction, spatial averaging is equivalent to increasing the total number of wave periods. In all tests, $M$ is about 25 and $N$ is 32, so the equivalent total number of periods is about 800, which is far more than the minimum of 50 periods suggested by Sleath (1987). The spatial- and phase-averaged velocity profile is finally Fourier analyzed to give the amplitude and phase profiles of individual harmonics. The phase-averaging, spatial-averaging and Fourier analysis may not necessary follow this sequence. For instance, in order to check the longitudinal uniformity, the phase-averaged velocity field is first Fourier analyzed. The results are then spatially averaged to give the standard deviations of amplitudes and phases, which indicate the variability, i.e. accuracy, of these measurements.

### Test conditions

The flow conditions presented in this paper are sinusoidal waves and sinusoidal waves combined with a current. Sinusoidal waves are specified by their radian frequency, $\omega$, and their near-bottom orbital velocity amplitude $U_{bm}$: $u(t)=U_{bm}\cos(\omega t)$.The current is specified by the pump rotation frequency. In this paper, it is set to 40Hz for most of the tests. This corresponds to a cross-section average velocity near the pump's design limit of about 50cm/s velocity in the test section. Two types of bottom roughness are used. One consists of smooth aluminum plates, resulting in smooth turbulent flow. The other is a mono-layer of 12.5mm-diameter ceramic balls. This roughness corresponds to fully rough turbulent flow. The ceramic balls are carefully placed and glued onto aluminum plates. Figure 2 shows the side view and top view of the rough bottom. The details of all test conditions are presented in Table 2. The Reynolds number of all tests with waves are of $O(10^6)$.

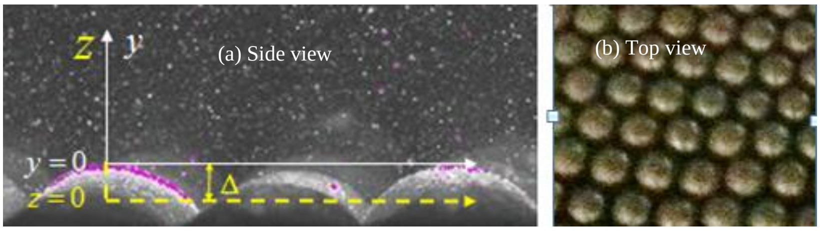


**Figure 2.Bottom covered with the ceramic balls (the side view is part of the actual PIV image)**

**Table 2. Summary of test conditions**

| Test ID | Flow type | Bottom type | Target $U_{bm}$ [cm/s] | $T$ [s] | Approx. $u_c$ [cm/s] | RE |
|---|---|---|---|---|---|---|
| SP400Ar | Wave | Rough | 157.1 | 6.25 | - | $3.1\cdot10^6$ |
| SP400Br | Wave | Rough | 78.5 | 12.5 | - | $1.6\cdot10^6$ |
| SP250r | Wave | Rough | 98.2 | 6.25 | - | $1.2\cdot10^6$ |
| SP200r | Wave | Rough | 39.3 | 12.5 | - | $0.4\cdot10^6$ |
| WC400Ar | Wave-current | Rough | 157.1 | 6.25 | 50 | $3.1\cdot10^6$ |
| WC400Br | Wave-current | Rough | 78.5 | 12.5 | 50 | $1.6\cdot10^6$ |
| WC250r | Wave-current | Rough | 98.2 | 6.25 | 50 | $1.2\cdot10^6$ |
| C40r | Current | Rough | - | - | 50 | - |
| C13r | Current | Rough | - | - | 17 | - |
| SP400As | Wave | Smooth | 157.1 | 6.25 | - | $3.1\cdot10^6$ |
| SP250s | Wave | Smooth | 98.2 | 6.25 | - | $1.2\cdot10^6$ |
| WC400As | Wave-current | Smooth | 157.1 | 6.25 | 50 | $3.1\cdot10^6$ |
| WC250s | Wave-current | Smooth | 98.2 | 6.25 | 50 | $1.2\cdot10^6$ |
| C40s | Current | Smooth | - | - | 50 | - |

## EXPERIMENTAL RESULTS

### Spatial- and phase-averaged velocity profiles

The spatial- and phase-averaged velocity profiles are Fourier analyzed to give the profiles of the mean current and the first three harmonics' amplitudes and phases. Due to the bottom reflection of the laser sheet, i.e., the blurred zone very close to the top of ceramic balls in Figure 2a, the flow field below $y$=1mm generally has low signal-to-noise ratio and consequently a high percentage of erroneous measurements. This is also true for the smooth bottom tests. Therefore, only measurements above $y$=1mm are taken as valid. Figure 3 shows the profiles of the first- and third-harmonic amplitudes and phases of test SP400Ar, while the second-harmonic phase and the residual current are shown in Figure 4. The gray zone indicates the variation in the longitudinal direction with its width indicating the standard deviation obtained from spatial averaging of the Fourier analysis results of the phase-averaged flow field. Clearly, the variation is only of the order mm/s, which suggests excellent longitudinal uniformity.

As the bottom is approached, the first-harmonic amplitude first increases a little and then decreases rapidly after the overshoot. The first-harmonic phase generally increases approaching the bottom. At about *y*=1mm, the local velocity leads the free-stream velocity by about 22 degrees. The residual current is only of the order mm/s and randomly distributed around zero. This is because the two half cycles of a sinusoidal oscillation are completely symmetric. Therefore, no mean current should be expected. The second-harmonic amplitude is almost uniform (about 2.5cm/s) and its phase, as shown in Figure 4, does not have a meaningful structure as do the first- and third-harmonic phases. By symmetry, the second harmonic should not exist, so the existence of an unstructured second-harmonic is regarded as experimental noise. Compared to the residual current and the second harmonic, the third harmonic is clearly meaningful. The upper part of the third harmonic is about 2cm/s in amplitude. This is partly due to a small third-harmonic produced by the piston, as shown in Table 1, and is partly due to some experimental error, as suggested by the existence of a second-harmonic. Its overshoot, starting from *y*=30mm, reaches about 8cm/s and this magnitude cannot be explained by the boundary layer associated with the piston-generated third harmonic. The third-harmonic phase also is highly organized. Thus, the third harmonic must be due to some boundary layer processes. For oscillatory boundary layer flows in a OWT, it can be only explained by a time-varying eddy viscosity theory, e.g. Trowbridge and Madsen (1984).

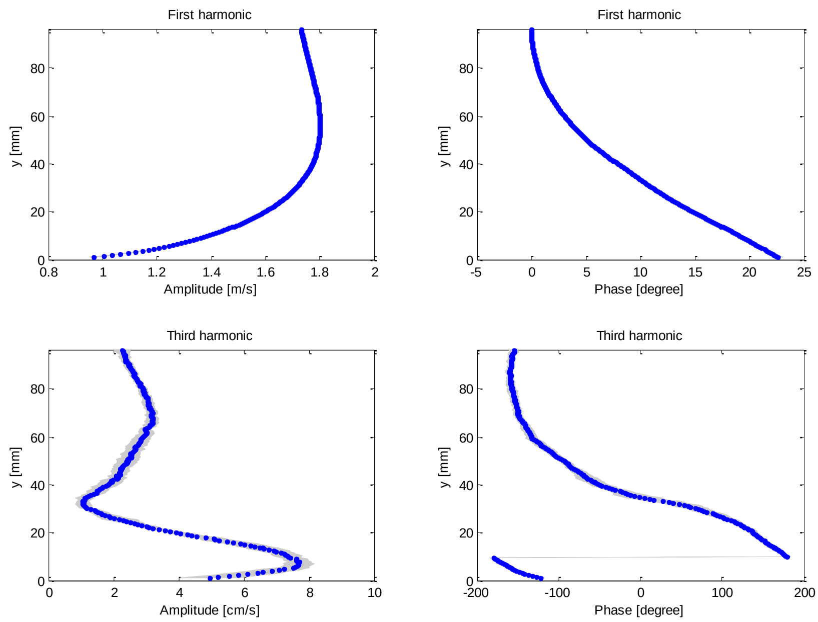


**Figure 3. Amplitudes and phases of the first and third harmonics (test SP400Ar)**

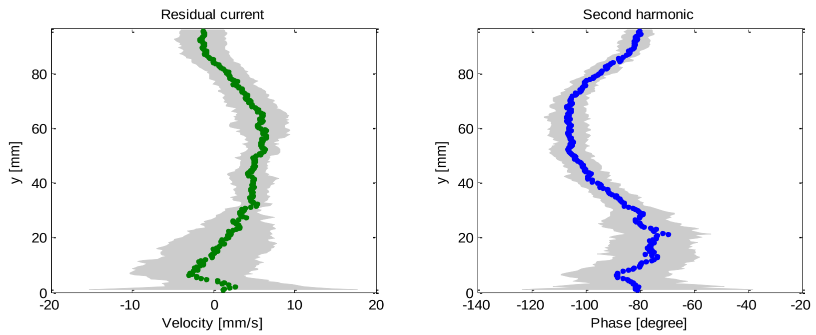


**Figure 4. Residual current and second-harmonic phase (test SP400Ar)**

## Log-profile fitting

For steady turbulent flow, it has been shown that the velocity profile can be approximated by a logarithmic profile. Many theoretical and experimental studies of wave boundary layers suggest that the log-profile can also be used for oscillatory boundary layers. For example, Grant and Madsen (1979) assumed a time-invariant eddy viscosity and obtained an analytical solution in terms of Kelvin functions of zeroth order, which they showed to reduce to a logarithmic velocity profile in the very near-bottom region:

$$u(z,t) = \frac{u_{*w}}{\kappa} \ln \frac{z}{z_0} \cos(\omega t + \varphi) \tag{4}$$

where $\kappa$ is the von Kármán constant, $z_0$ is the roughness height, $u_{*w}$ is the shear velocity, and $\varphi$ is phase difference between the near-bottom velocity and the free-stream velocity. This log-profile approximation is only valid in the region very close to the bottom, i.e. the normalized vertical coordinate $\xi=z/l$ must be small. Here $l$ is a characteristic length scale of the oscillatory bottom boundary layer:

$$l = \frac{\kappa u_{*w}}{\omega} \tag{5}$$

Eq. (4) suggests that the velocity amplitude profile also follows the log law. Thus, it can be written as:

$$U(z) = \frac{u_{*w}}{\kappa} \ln \frac{y+\Delta}{z_0} \tag{6}$$

Here Δ, as shown in Figure 2, is the zero offset that relates the hydrodynamic vertical coordinate $z$ to an author-defined vertical coordinate $y$, for which we chose the origin at the top of the bottom roughness element. For rough bottom tests, this offset is clearly an unknown. To quantify it, different values of Δ between zero and one ceramic ball diameter (12.5mm) were tried in the log-profile fitting. The optimal value of Δ is the one which gives the best log-profile fitting property, i.e., the coefficient of determination $R^2$ closest to unity. The first-harmonic amplitude profiles of all the pure sinusoidal wave tests are used to search for Δ. In additional, two pure current tests with the pump rotating at 40Hz and 13Hz are also included. Table 3 shows the summary of the results. The pure current flows and pure wave flows give virtually the same zero offset. This suggests that the zero offset has no dependency on flow conditions if the flow is fully rough turbulent. The obtained Δ is about 4mm, which is about 32% of the ceramic ball diameter, with 0.4mm standard deviation. This is very close to the Δ $=0.29D_{50}$ reported by van der A et al. (2011), who used a mono-layer of rounded natural gravels (diameter between 5mm to 6.3mm) glued onto marine graded plywood as roughness elements. One possible reason for the 0.4mm uncertainty is that the ceramic balls are not completely homogenous. They are handmade, so their diameters could have some slight variation. However, 0.4mm uncertainty is merely 10% of the 4mm mean value, i.e. negligible. Hereafter, the zero offset Δ for all rough bottom tests is taken as 4mm.

**Table 3. Zero offset given by log-profile fitting**

| Test ID | Min(1-$R^2$) | Δ [*mm*] |
|---|---|---|
| SP400Ar | $8.8\cdot10^{-5}$ | 3.6 |
| SP400Br | $5.4\cdot10^{-5}$ | 3.8 |
| SP250r | $3.9\cdot10^{-5}$ | 4.3 |
| SP200r | $2.1\cdot10^{-4}$ | 4.5 |
| C40r | $5.9\cdot10^{-5}$ | 4.4 |
| C13r | $1.1\cdot10^{-4}$ | 3.6 |

As mentioned before, the log-profile is a good approximation only in the very near-bottom region: $\xi=z/l<\varepsilon$ ($\varepsilon<<1$). In order to have a sufficient number of data points for log-profile fitting (ideally more than 10), the value of $\varepsilon$ is set to 0.15. This is the upper limit for selecting data. Calculating the characteristic length scale $l$ needs a shear velocity, which can only be determined after the log-profile fitting. Therefore, iterations are needed to select the appropriate data points. Due to the poor signal-to-noise ratio of PIV measurements, the lower limit for acceptable data is y=1mm, i.e. 1mm or more above the top of roughness elements. Thus, for rough bottom tests only measurements for $z=y+\Delta>5$mm are used in the log-profile fitting. These two rules for data selection were also applied when searching for the optimal value of the zero offset Δ.

Figure 5 shows the log-profile fitting to the first-harmonic amplitude in test SP400Ar. The green circles indicate the selected measurements, while the solid line is the fitted log-profile. The shear velocity obtained from the log-fit is 17.6cm/s, with 95% confidence intervals of merely ±0.9%. The corresponding bottom roughness ($k_N$=$30z_0$) is 16.8mm, which is comparable to the ceramic ball diameter, and a 95% confidence interval of ±11.1%. These confidence limits suggest extra-ordinarily accurate determination of the shear velocity and the bottom roughness. Table 4 summarizes results from log-profile fitting for other rough bottom tests. The obtained roughness is generally around 20mm with 95% confidence intervals of about ±10%, except for test SP200r. This is because test SP200r has the thinnest boundary layer, so it has the fewest data points (only 5) satisfying the rules for data selection. The consistency of the obtained roughness values suggests that this is independent on flow conditions, so long as the flow is fully developed rough turbulent.

Since the shear velocity is given by $u_{*w}=\sqrt{f_w/2}U_{bm}$, where $f_w$ is the wave friction factor introduced by Jonsson (1966), the obtained shear velocities can be compared with predictions by Madsen (1994), who presented explicit approximations for the wave friction factor,

$$f_w=\begin{cases}\exp(7.02\dfrac{A_{bm}}{k_N}^{-0.078}-8.82) & 0.2<\dfrac{A_{bm}}{k_N}<10^2\\ \exp(5.61\dfrac{A_{bm}}{k_N}^{-0.108}-7.30) & 10^2<\dfrac{A_{bm}}{k_N}\end{cases} \tag{7}$$

and for the phase lead of the bottom shear stress,

$$\varphi[°]=33-6.0\log_{10}(\frac{A_{bm}}{k_N}) \qquad \frac{A_{bm}}{k_N}<10^3 \tag{8}$$

Using Eq. (7) and 20mm for the bottom roughness, the estimated shear velocities are shown in the last column of Table 4. The predicted shear velocities are always slightly smaller (by less than 10%) than those obtained experimentally. The reason for this discrepancy is likely that Madsen (1994) did not include time variation of eddy viscosity in his model.

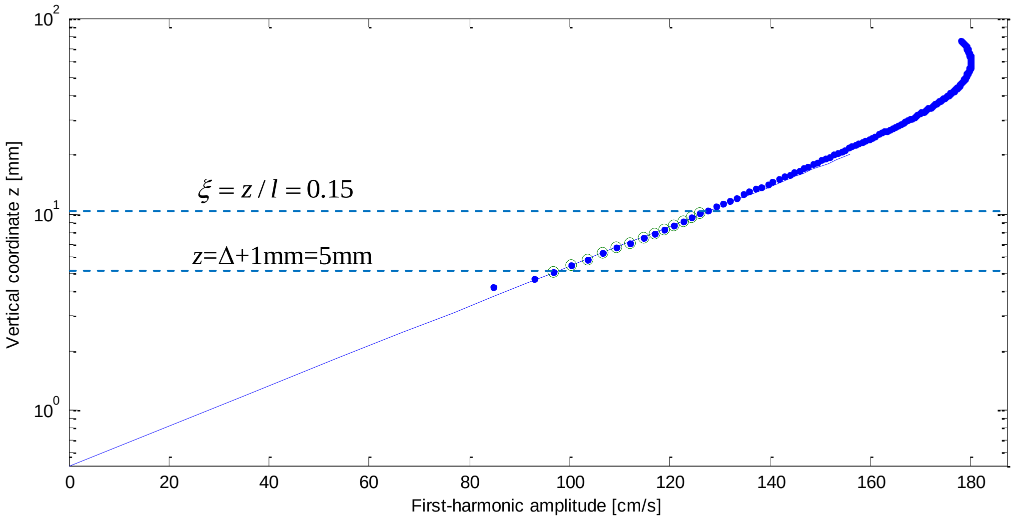


**Figure 5. Log-profile fitting to the first-harmonic amplitude of test SP400Ar**

| **Table 4. Log-profile fitting to the tests over the rough bottom** | | | | | | |
|---|---|---|---|---|---|---|
| Test ID | 1-$R^2$ | $u_*$[cm/s] | ±$\Delta u_*/u_*$ | $k_N$[mm] | ±$\Delta k_N/k_N$ | $u_{*w,predicted}$[cm/s] |
| SP400Ar | $1.2\cdot10^{-4}$ | 17.6 | 0.9% | 16.8 | 11.1% | 17.5 |
| SP400Br | $8.1\cdot10^{-5}$ | 9.5 | 0.6% | 22.8 | 6.9% | 8.7 |
| SP250r | $7.5\cdot10^{-5}$ | 13.2 | 0.9% | 20.8 | 10.7% | 12.2 |
| SP200r | $2.7\cdot10^{-4}$ | 5.4 | 2.3% | 22.5 | 28.2% | 4.9 |
| C40r | $9.8\cdot10^{-5}$ | 3.5 | 0.3% | 19.7 | 3.1% | - |

For smooth bottom tests, due to the strong bottom reflection, the PIV image of the bottom is a very bright layer of about 10 pixels (0.5mm), i.e. the pink layer in Figure 6. The actual bottom location is hiding inside this thin layer, so the zero offset Δ is still unknown. Since the bottom is smooth, the boundary layer thickness is much thinner than that for rough bottom tests. This reduces the amount of available data points for log-profile fitting. Thus, the uncertainty of log-profile fitting becomes much more significant. For example, the 95% confidence interval of the fitted roughness can be more than 50%, e.g., test SP400As. This considerable experimental uncertainty makes it impossible to determine such a small Δ (less than 0.5mm) by log-profile fitting the wave amplitude profiles or the current profiles. Nikuradse (1933) showed that the equivalent bottom roughness for steady smooth turbulent flows is:

$$k_N = 3.3\nu / u_* \tag{9}$$

Thus, there are two ways to obtain the bottom roughness using log-profile fitting of current velocity profiles: one is directly from log-profile fitting and the other is calculated using this formula and the fitted shear velocity. The optimal value of Δ is the one which gives identical roughness values. Based on several pure current tests, the Δ is found to be 0.15mm (3 pixels) with an uncertainty less than 1 pixel. Using the obtained Δ, the log-profile fitting of one pure current test (test C40s) is shown in Table 5. The fitted roughness (0.14mm) is very close to the prediction (0.15mm) as expected.

The validity of using Eq. (9) for smooth oscillatory boundary layer flow has not been proved. Also, which representative shear velocity to use for unsteady flows is unknown. Table 5 shows the results of log-profile fitting of two pure wave tests with the last column showing the predictions of the bottom roughness using Eq. (9). The shear velocities used are those obtained by log-profile fitting of first-harmonic amplitude profiles, i.e., the shear velocity based on maximum shear stress. For test SP400As and SP250s, the predicted roughness and the fitted roughness are in reasonable agreement. Another possible choice of shear velocity to use in Eq. (9) for oscillatory flows is the period-average shear velocity. This might be a more reasonable choice because it represents the mean turbulence level. However, due to the considerable uncertainty of the fitted roughness, it is not possible to conclude which shear velocity should be chosen using these results. Nevertheless, our study demonstrates the general validity of Eq. (9) conclusively for both steady and unsteady oscillatory flows.

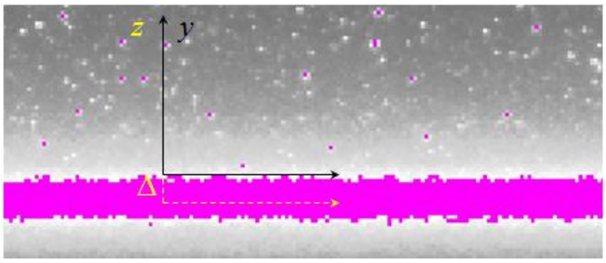


**Figure 6. PIV image of the smooth bottom**

**Table 5. Log-profile fitting to tests over the smooth bottom**

| Test ID | $1-R^2$ | $u_*$[cm/s] | $\pm\Delta u_*/u_*$ | $k_N$[mm] | $\pm\Delta k_N/k_N$ | $k_N=3.3\nu/u_{*w}$ [mm] |
|---|---|---|---|---|---|---|
| SP400As | $1.4\cdot10^{-3}$ | 7.3 | 3.6% | $4.7\cdot10^{-2}$ | 73.3% | $3.6\cdot10^{-2}$ |
| SP250s | $3.6\cdot10^{-4}$ | 4.5 | 2.2% | $3.2\cdot10^{-2}$ | 44.2% | $5.8\cdot10^{-2}$ |
| C40s | $2.3\cdot10^{-4}$ | 1.7 | 0.6% | 0.14 | 11.1% | 0.15 |

### Shear stress from momentum integral

Integrating the linearized momentum equation for oscillatory boundary layer flows is one way to obtain the bottom shear stress:

$$\tau(z,t) = \int_z^{z_\infty} \frac{\partial(u_\infty - u)}{\partial t} dz \tag{10}$$

Here $z_\infty$ is where the deficit velocity $u_\infty$-$u$ vanishes. For most tests, the highest level of PIV measurements can be used as $z_\infty$. Eq. (10) is Fourier analyzed to give the complex amplitude of the nth-harmonic shear stress:

$$\tau^{(n)}(z) = \int_z^{z_\infty} in\omega(U_\infty^{(n)} - U^{(n)}) dz \tag{11}$$

where $U^{(n)}$ is the complex amplitude of the nth-harmonic velocity. This integral stops at the lower boundary of the measured area $z=z_{\min}$=5mm. To extrapolate it down to the bottom, it is assumed that the amplitude profile between $z=z_0$ and $z=z_{\min}$ follows the log profile and the phase is constant, as suggested by Eq. (4). Therefore, the shear stress is easily extrapolated to the bottom by adding:

$$\int_{z_0}^{z_{\min}} in\omega(U_\infty^{(n)} - U^{(n)})dz = in\omega\{U_\infty^{(n)}(z_{\min} - z_0) - U^{(n)}(z_{\min})[z_{\min} - (z_{\min} - z_0)/\ln(\frac{z_{\min}}{z_0}]\} \quad (12)$$

The corresponding shear velocity is:

$$u_{*w}{}^{(n)} = \sqrt{|\tau_b{}^{(n)}|/\rho} \quad (13)$$

And the phase lead of the bottom shear stress related to the free-stream velocity is:

$$\varphi^{(n)} = Arg(\tau_b{}^{(n)}) \quad (14)$$

Table 6 shows the obtained shear velocities and phase leads of the first-harmonic bottom shear stress from the momentum integral. The corresponding results given by the log-profile fitting and the Madsen (1994) model are also presented for comparison. The phase lead given by log-profile fitting is just the phase of the measured first-harmonic velocity closest to the bottom, since Eq. (4) suggests that the phase is constant in the near-bottom region. In general, the three approaches give similar results for the shear velocities and phase leads. The agreement of phase leads is good. The discrepancy is generally less than 3 degrees. The momentum integral gives smaller amplitudes of shear velocities than the log-profile fitting and the predictions by Madsen (1994) model. Similar results have been reported by van der A et al. (2011). They claimed that the differences are due to a small longitudinal variation of the flow field, i.e., a non-vanishing $\partial(uu)/\partial x$. However, our measurements have shown very good uniformity in the longitudinal direction and the spatial-average should also remove this effect, so this is unlikely to be the reason. Since most contribution to the momentum integral is from the near-bottom region where the velocity profile changes rapidly, in order to have high accuracy of the integral, it is necessary to have measurements as close to the theoretical bottom location $z$=0 as possible. For rough bottom tests, there is a roughly 5mm blank region from the lower level where valid measurements exist to the theoretical bottom location $z$=0. Since there is no measurement at all, a fictitious log-profile distribution is assumed to extrapolate the momentum integral to the bottom. This may carry some noticeable error. Another possible reason is the vertical resolution is not fine enough, so the numerical integral deviates from the true value. The actual reason is still uncertain. Future studies are needed to reveal the underlying reason for the difference between the shear velocity estimations afforded by these two approaches.

**Table 6. Shear velocities and phase leads of the bottom shear stress**

| Test ID | Momentum integral | | Log-profile fitting | | Madsen (1994) | |
|---|---|---|---|---|---|---|
| | $u_{*w}$ [cm/s] | $\varphi$[°] | $u_{*w}$ [cm/s] | $\varphi$[°] | $u_{*w}$ [cm/s] | $\varphi$[°] |
| SP400Ar | 14.5 | 24.4 | 17.6 | 22.2 | 17.5 | 21.4 |
| SP400Br | 7.0 | 25.0 | 9.5 | 22.6 | 8.7 | 21.4 |
| SP250r | 9.4 | 20.3 | 13.2 | 22.5 | 12.2 | 22.8 |
| SP200r | 3.6 | 26.8 | 5.4 | 23.8 | 4.9 | 23.4 |
| SP400As | 7.0 | 12.3 | 7.5 | 12.3 | 7.7 | 9.9* |
| SP250s | 4.3 | 14.4 | 4.5 | 13.0 | 5.2 | 10.2* |

*used the original solution by Grant and Madsen (1979) since it is outside the applicable range of Eq. (8)

### The combined wave-current boundary layer

When waves and currents co-exist, the wave boundary layer has much shorter time to develop and it is therefore much thinner than the current boundary layer. Grant and Madsen (1979) suggested that inside the wave boundary layer the turbulent eddy viscosity should be scaled with a combined shear velocity $u_{*wc}$ which is based on the maximum bottom shear stress, but outside the wave boundary layer the eddy viscosity is simply scaled with the current shear velocity $u_{*c}$. Therefore, they assumed a two-layer time-invariant eddy viscosity $\nu_T$ :

$$\nu_T = \begin{cases} \kappa u_{*wc} z & z < \delta \\ \kappa u_{*c} z & z > \delta \end{cases} \quad (15)$$

with:

$$u_{*wc} = \sqrt{|\tau_{bc} + \tau_{bw}|/\rho}$$

$$u_{*c} = \sqrt{|\tau_{bc}|/\rho}$$

$$\delta = A \cdot \kappa u_{*wc} / \omega$$

where $\tau_{bc}$ is the current bottom shear stress and $\tau_{bw}$ is the maximum wave bottom shear stress. The coefficient $A$ was originally taken as 2 by Grant and Madsen (1979), but has later been shown to be a function of the relative roughness, $A_{bm}/k_N$. However, in the present context, the actual value of $A$ is immaterial. The nonlinear wave-current interaction is considered by the definition of the combined wave-current shear velocity $u_{*wc}$. Using this simple eddy viscosity model, they showed that the current velocity profile has a two-log-profile structure:

$$u_c(z) = \begin{cases} = \dfrac{{u_{*c}}^2}{\kappa u_{*wc}} \ln \dfrac{z}{z_0} & z < \delta \\ = \dfrac{u_{*c}}{\kappa} \ln \dfrac{z}{z_{0a}} & z > \delta \end{cases} \tag{16}$$

The most significant finding is that the upper part of the current profile is controlled by an apparent roughness $k_{Na}=30z_{0a}$ which is much larger than the physical roughness $k_N=30z_0$. This finding explained why some field studies gave unrealistically large roughness after log-profile fitting the measured current profile (Forristall et al., 1977). This is because all the measurements are within the upper layer, so the obtained roughness is the apparent roughness. Since the lower part of the profile only exists inside the thin wave boundary layer, very few high quality field or laboratory measurements of the lower part of the current profile are available.

Figure 7 shows the measured current velocity profile and the first-harmonic amplitude profile of test WC400Ar. The current profile is very similar to the conceptual two-log-profile, except that there is a smooth transition between the two straight lines. This is because the Grant and Madsen (1979) model uses a discontinuous eddy viscosity. The results of log-profile fittings are shown in Table 7. The first-harmonic amplitude profile is first fitted using the data selection rules described before. The same data points are used in fitting the lower current profile. The two log-profile fittings give similar roughness (11.3mm and 11.9mm). The obtained roughness is of the same order as the ceramic ball diameter, but is somewhat smaller than the value found from pure sinusoidal wave and pure current tests (Table 3). The wave shear velocity is 15.7cm/s, and the shear velocity of the lower current profile is 2.9cm/s. This shear velocity, as suggested in Eq. (16) is determined by the actual current shear velocity and the wave shear velocity. Therefore, the actual current shear velocity can be obtained by solving the following equation:

$$2.9cm/s = \frac{{u_{*c}}^2}{\sqrt{{u_{*c}}^2 + (15.7cm/s)^2}}$$

The result is 7.1cm/s. The log-profile fitting of the upper current profile shows that the apparent roughness is 186.5mm. This is, as indicated by the theory, much larger than the physical roughness. The fitted current shear velocity is 8.3cm/s, which is a bit larger than the one deduced from the lower current profile. This difference and the underestimation of the physical roughness could be due to some unconsidered physics in the Grant-Madsen (1979) model, such as the time-variation of eddy viscosity.

**Table 7. Log-profile fitting to the current velocity profile and the first-harmonic amplitude profile of Test WC400Ar**

| | $1-R^2$ | $u_*$[cm/s] | $\pm\Delta u_*/u_*$ | $k_N$[mm] | $\pm\Delta k_N/k_N$ |
|---|---|---|---|---|---|
| Current (lower part) | 1.9·10-3 | 2.9 | 4.4% | 11.3 | 57.6% |
| Current (upper part) | 1.5·10-3 | 8.3 | 0.8% | 186.5 | 5.8% |
| Wave | 2.6·10-4 | 15.7 | 1.6% | 11.9 | 20.7% |

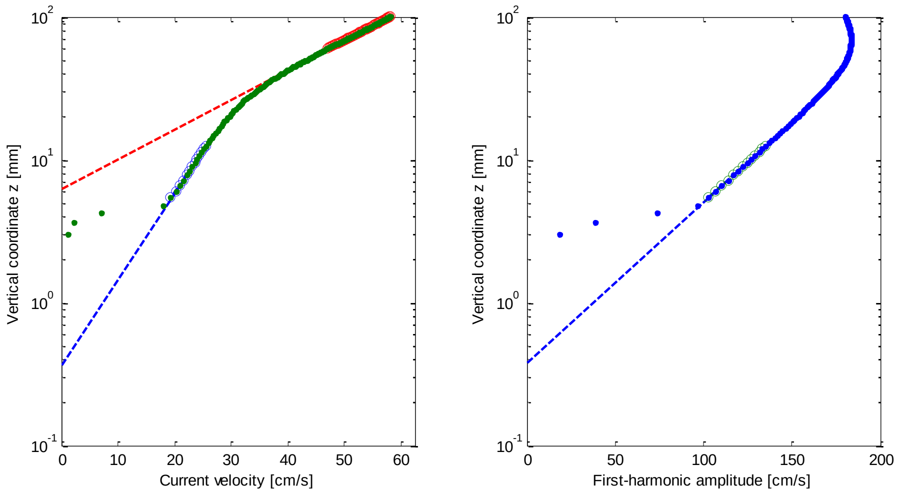


**Figure 7. Vertical profiles of the current velocity and the first-harmonic amplitude of test WC400Ar (dashed lines: fitted log profiles; circles: selected data points for log-profile fitting; dots: measurements)**

## CONCLUSIONS

A new OWT has been built in the Hydraulic Laboratory of the Civil and Environmental Department at the National University of Singapore. It can accurately produce any desired wave form (sinusoidal, nonlinear, random waves, etc.), as well as combined wave-current flow. High quality PIV measurements of wave and combined wave-current boundary layers over smooth and rough bottoms were obtained. The spatial- and phase-averaged velocity is Fourier analyzed to give profiles of amplitudes and phases.

Experimental results show that the logarithmic profile can accurately approximate the near-bottom first-harmonic amplitude of sinusoidal waves. For rough bottom tests, the log-profile fitting give highly accurate determinations of the hydrodynamic roughness and the theoretical bottom location with only about 10% uncertainty. Smooth bottom tests demonstrate that the equivalent bottom roughness formula for steady smooth turbulent flow suggested by Nikuradse (1993), $k_N=3.3\nu/u_*$, is also applicable for smooth turbulent oscillatory flow. The fitted shear velocities and measured near-bottom phase leads can be quite accurately predicted by the Madsen (1994) model.

The momentum integral method gives smaller shear velocities than the log-profile fitting and the Madsen (1994) model, but the agreement is still reasonable. The discrepancy is possibly due to some error when extrapolating the integral to the bottom. However, the phase leads afforded by it agree well with the observed near-bottom phase leads and the Madsen (1994) model's predictions.

The current profile of the combined wave-current flow indicates a two-logarithmic-profile structure as suggested by simple combined wave-current turbulent boundary layer models, e.g. Grant and Madsen (1979). An apparent roughness which is much larger than the physical roughness is observed. The current shear velocity deduced from the lower current profile using the Grant and Madsen (1979) theory agrees reasonably well with the one obtained from log-profile fitting the upper current profile. The difference between the two current shear velocities, as well as a small but meaningful third harmonic embedded in a pure sinusoidal wave, suggest the existence of a time-varying turbulent eddy viscosity.

## Acknowledgments

We gratefully acknowledge the financial support for this research from the National Research Foundation of Singapore (NRF) through the Singapore-MIT Alliance for Research and Technology's (SMART) Center for Environmental Sensing and Modeling (CENSAM) program.

## REFERENCES

Dohmen-Janssen, C. M. and D. M. Hanes. 2002. Sheet flow dynamics under monochromatic nonbreaking waves, *J. Geophys. Res.*, 107(C10), 3149.

Dohmen-Janssen, C. M., W. N. Hassan, et al. 2001. Mobile-bed effects in oscillatory sheet flow, *J. Geophys. Res.*, 106(C11), 27103-27115.

Dohmen-Janssen, C. M., D. F. Kroekenstoel, et al. 2002. Phase lags in oscillatory sheet flow: experiments and bed load modelling, *Coastal Engineering*, 46(1), 61-87.

Forristall, G. Z., R. C. Hamilton, et al. 1977. Continental Shelf Currents in Tropical Storm Delia: Observations and Theory, *Journal of Physical Oceanography*, 7(4), 532-546.

Grant, W. D. and O. S. Madsen. 1979. Combined Wave and Current Interaction With a Rough Bottom, *J. Geophys. Res.*, 84(C4), 1797-1808.

Hino, M., M. Kashiwayanagi, et al. 1983. Experiments on the turbulence statistics and the structure of a reciprocating oscillatory flow, *Journal of Fluid Mechanics*, 131, 363-400.

Jensen, B. L., B. M. Sumer, et al. 1989. Turbulent oscillatory boundary layers at high Reynolds numbers, *Journal of Fluid Mechanics*, 206, 265-297.

Jonsson, I. G. 1966. Wave boundary layer and friction factors. *the 10th conference on Coastal Engineering*, Tokyo, ASCE. 127-148

Jonsson, I. G. and N. A. Carlsen. 1976. Experimental and theoretical investigations in an oscillatory turbulent boundary layer, *Journal of Hydraulic Research*, 14(1), 45-60.

Madsen, O. S. 1994. Spectral wave-current bottom boundary layer flows. *the 24th International Conference on Coastal Engineering*, ASCE. 384-398

Nikuradse, J. 1933. Stroemungsgesetze in rauhen Rohren, *Ver. Dtsch. Ing. Forsch.*, 361.

Sleath, J. F. A. 1987. Turbulent oscillatory flow over rough beds, *Journal of Fluid Mechanics*, 182, 369-409.

van der A, D. A., T. O'Donoghue, et al. 2011. Experimental study of the turbulent boundary layer in acceleration-skewed oscillatory flow, *Journal of Fluid Mechanics*, 684, 251-283.